environmental microbiology

Environmental Microbiology (2013) **15**(4), 1063–1077 doi:10.1111/1462-2920.12029

# Fungal oxidative dissolution of the Mn(II)-bearing mineral rhodochrosite and the role of metabolites in manganese oxide formation

**Yuanzhi Tang,[1†] Carolyn A. Zeiner,[1†] Cara M. Santelli[2] and Colleen M. Hansel[1‡*]**

[1]*School of Engineering and Applied Sciences, Harvard University, Cambridge, MA, USA.*

[2]*Department of Mineral Sciences, National Museum of Natural History, Smithsonian Institution, Washington, DC 20560, USA.*

## Summary

**Microbially mediated oxidation of Mn(II) to Mn(III/IV) oxides influences the cycling of metals and remineralization of carbon. Despite the prevalence of Mn(II)-bearing minerals in nature, little is known regarding the ability of microbes to oxidize mineral-hosted Mn(II). Here, we explored oxidation of the Mn(II)-bearing mineral rhodochrosite ($MnCO_3$) and characteristics of ensuing Mn oxides by six Mn(II)-oxidizing Ascomycete fungi. All fungal species substantially enhanced rhodochrosite dissolution and surface modification. Mineral-hosted Mn(II) was oxidized resulting in formation of Mn(III/IV) oxides that were all similar to δ-$MnO_2$ but varied in morphology and distribution in relation to cellular structures and the $MnCO_3$ surface. For four fungi, Mn(II) oxidation occurred along hyphae, likely mediated by cell wall-associated proteins. For two species, Mn(II) oxidation occurred via reaction with fungal-derived superoxide produced at hyphal tips. This pathway ultimately resulted in structurally unique Mn oxide clusters formed at substantial distances from any cellular structure. Taken together, findings for these two fungi strongly point to a role for fungal-derived organic molecules in Mn(III) complexation and Mn oxide templation. Overall, this study illustrates the importance of fungi in rhodochrosite dissolution, extends the relevance of biogenic superoxide-based Mn(II) oxidation and highlights the potential role of mycogenic exudates in directing mineral precipitation.**

Received 19 August, 2012; revised 11 October, 2012; accepted 15 October, 2012. *For correspondence. E-mail chansel@whoi.edu; Tel. (+1) 508 289 3858; Fax (+1) 508 457 2161. †These authors contributed equally to this work. ‡Present address: Marine Chemistry and Geochemistry Department, Woods Hole Oceanographic Institution, Woods Hole, MA 02543, USA.

## Introduction

Mn(III, IV) oxides are ubiquitous in the environment, including terrestrial and aquatic systems. Due to their small particle size, large surface area and high sorptive and oxidative capacities, Mn oxides are among the most reactive mineral phases in the environment. They influence a variety of biogeochemical reactions, such as the degradation of organic matter (Stone and Morgan, 1984; Sunda and Kieber, 1994), cycling of metals (Murray and Tebo, 2007; Murray *et al*., 2007; Lafferty *et al*., 2010) and anaerobic respiration coupled to carbon oxidation (Nealson and Saffarini, 1994). The majority of natural Mn oxides are thought to be formed from either direct or indirect microbial Mn(II) oxidation (Tebo *et al*., 2004). A large diversity of Mn(II)-oxidizing bacteria and fungi have been identified in a wide range of ecological niches spanning from desert sediments to surface marine waters (de la Torre and Gomez-Alarcon, 1994; Tebo *et al*., 2005; Hansel and Francis, 2006; Miyata *et al*., 2006a; 2007; Cahyani *et al*., 2009; Santelli *et al*., 2010). At present, Mn(II)-oxidizing fungi are limited to the phyla Ascomycota and Basidomycota, where Basidiomycota (specifically the wood rotting fungi) have received considerably more attention due to their importance in the degradation of lignin. Recently, we have discovered an abundant and diverse group of Mn(II)-oxidizing Ascomycota within Mn-laden treatment systems (Santelli *et al*., 2010) and a freshwater lake (C.M. Santelli, unpublished).

While Mn(II) oxidation to Mn(III) has been extensively studied for Basidiomycota, the mechanisms and pathways of Mn(II) oxidation by Ascomycota are poorly understood. The primary enzymes implicated in Mn(II) oxidation are manganese peroxidases by Basidiomycete fungi (Glenn *et al*., 1986; Wariishi *et al*., 1992) and laccases or laccase-like metalloproteins in Ascomycetes (Hofer and Schlosser, 1999; Schlosser and Hofer, 2002; Miyata *et al*., 2004). Recently, extracellular superoxide ($O_2^-$) has been identified as the oxidant of Mn(II) to Mn(III) in the common Ascomycete fungus *Stilbella aciculosa* (Hansel *et al*., 2012). Surprisingly, superoxide-mediated Mn(II) oxidation has also

recently been discovered for the marine bacterium *Roseobacter* sp. Azwk-3b (Learman *et al*., 2011a), revealing an unforeseen homology in fungal and bacterial Mn(II) oxidation pathways. In fact, these findings are consistent with thermodynamic modelling of Mn(II) oxidation reactions indicating that while the oxidation of Mn(II) to Mn(III) by oxygen is thermodynamically prohibited, oxidation by superoxide is thermodynamically favourable over all relevant pH ranges (Luther, 2010). In fact, superoxide was found to be a rapid oxidant of Mn(II) in natural seawater and following photoexcitation of humic substances (Nico *et al*., 2002; Hansard *et al*., 2011). The production of extracellular reactive oxygen species (ROS), and particularly that of superoxide, is widespread throughout the fungal kingdom (Bedard *et al*., 2007), where it is employed for various physiological processes, including the regulation of cell differentiation (Takemoto *et al*., 2007) and apical dominance in hyphal growth (Semighini and Harris, 2008). However, the prevalence of a ROS-mediated Mn(II) oxidation mechanism in fungi is unknown.

Both enzymatic and superoxide-mediated Mn(II) oxidation are one electron transfer reactions leading to the formation of Mn(III) (Glenn *et al*., 1986; Hofer and Schlosser, 1999; Hansard *et al*., 2011). The fate of Mn(III) and processes responsible for subsequent formation of Mn oxides are unknown. Mn(III) may be further oxidized or may disproportionate leading to Mn(IV) production and spontaneous precipitation of Mn oxides. Due to the instability of Mn(III) in the absence of stabilizing ligands (Kostka *et al*., 1995; Klewicki and Morgan, 1998; 1999; Luther *et al*., 1998), either exogenous or endogenous organic molecules may be important in the formation of Mn oxides following microbial Mn(II) oxidation. In fact, protein and polysaccharide polymers have been identified underlying Mn oxides produced by a *Pedomicrobium*-like bacterium (Ghiorse and Hirsch, 1979) and an unidentified Basidiomycete fungus (Emerson *et al*., 1989), where they possibly play a mechanistic role in Mn oxide formation. Recent studies have also shown that organic molecules and specifically proteins may serve as mineral nucleation sites to facilitate particle aggregation in the biomineralization of zinc, iron, cadmium, and selenium (Moreau *et al*., 2007; Chan *et al*., 2011; Chen *et al*., 2011; Lenz *et al*., 2011). Collectively, the mechanisms responsible for the oxidation of Mn(II) and ultimate formation of Mn oxides by Ascomycete fungi as well as within the environment are poorly understood.

Despite the large variety of natural and synthetic Mn oxides known to exist (over 30), the predominant form of biogenic Mn oxides formed at circumneutral pH is a highly disordered, nanocrystalline, phyllomanganate phase, similar to hexagonal birnessite (Villalobos *et al*., 2003; Bargar *et al*., 2005; Webb *et al*., 2005). This phase is highly reactive and can undergo abiotic transformation and ripening to form more ordered and crystalline phases such as todorokite, feitknechtite, and triclinic birnessite (Bargar *et al*., 2005; Feng *et al*., 2010; Learman *et al*., 2011b). Within the natural environment, Ascomycete fungi generally grow attached to substrates, particularly minerals, yet most exploration of Mn(II) oxidation by Ascomycete fungi has focused on growth in liquid media or on agar-solidified media (Miyata *et al*., 2006b; Cahyani *et al*., 2009; Petkov *et al*., 2009; Saratovsky *et al*., 2009; Santelli *et al*., 2011). In fact, Santelli and colleagues (2011) found that growth conditions (i.e. planktonic versus surface-attached growth) impacted the composition and structure of Mn oxides formed. Considering the widely observed role of fungi in the chemical and mechanical alteration of minerals (Gadd, 1999; 2007; Sterflinger, 2000), they are likely important weathering agents of Mn(II)-hosted minerals (Golden *et al*., 1992). Yet, little is known regarding the ability of fungi to oxidize mineral-hosted Mn(II), the mechanisms of oxidation, and the morphological and structural characteristics of the ensuing Mn oxides.

In this study, we examined the interaction of six Mn(II)-oxidizing fungal species with the mineral rhodochrosite ($MnCO_3$), a common Mn(II)-bearing mineral found in a wide range of environments including terrestrial soils and marine sediments. By combining chemical assays and a variety of microscopic and spectroscopic techniques, we examined the oxidation of rhodochrosite by six fungal species and the properties of the ensuing Mn oxides. For a subset of fungi, we also examined the mechanisms of Mn(II) oxidation and Mn oxide precipitation. Results from this study provide a better understanding of the mechanisms of rhodochrosite dissolution and alteration, the diverse characteristics of fungal Mn oxides, as well as the biogeochemical cycling of manganese in the environment.

## Results and discussion

### *Fungal alteration and oxidation of rhodochrosite*

Fungal growth on rhodochrosite surfaces resulted in the production of oxidized Mn, as Mn(III) and Mn(IV), and removal of aqueous Mn(II) (Fig. 1). Figure 1A shows the concentrations of Mn(II) and Mn(III/IV) produced after 22 days of reaction between rhodochrosite and each of the six fungal species employed in this study (see Table 1 for fungal species name). The relative percentages of the Mn(II) in solution and Mn(III/IV) produced following reaction, as compared with the initial total Mn provided (as $MnCO_3$), are shown in Fig. 1B. The control sample (rhodochrosite without fungi) contained ~ 45 μM Mn(II) in solution, accounting for ~ 7% of the total initial $MnCO_3$ present, owing to (abiotic) dissolution of rhodochrosite in the acetate-yeast extract (AY) medium. As evidenced by a lack of reaction with Leucoberbelin Blue (LBB), oxidized Mn as Mn(III/IV) species was not detected in the

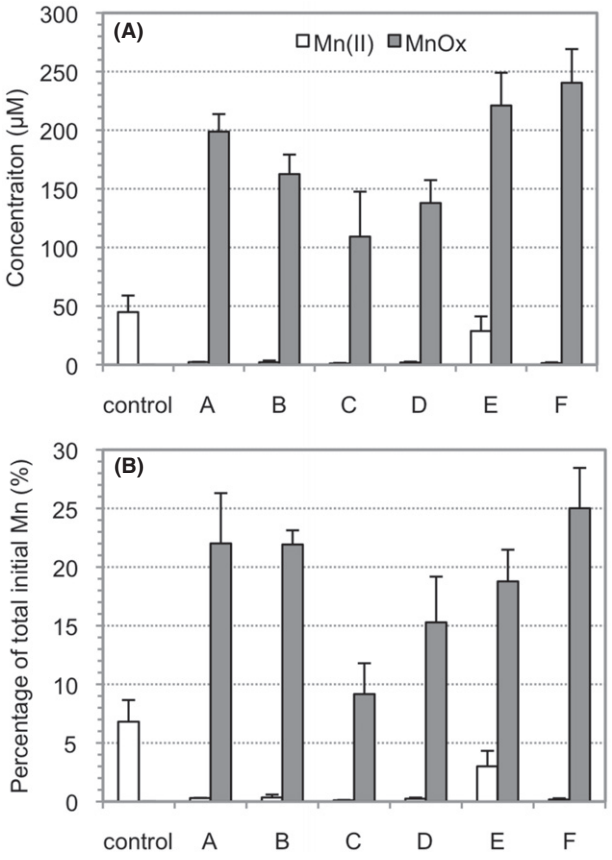


**Fig. 1.** (A) Concentration and (B) percentage of Mn(II) and Mn(III, IV) oxides of the total initial Mn added as $MnCO_3$ at day 22 for rhodochrosite reacted with fungal species A–F (see Table 1 for species name).

control sample, consistent with the thermodynamic inhibition of Mn(II) oxidation by molecular oxygen (Luther, 2005) and slow reaction kinetics of mineral-catalysed Mn(II) oxidation under these conditions (Diem and Stumm, 1984). On the contrary, the growth of all six fungal species caused a significant decrease in dissolved Mn(II) concentrations in the growth medium (below 2 μM for all species except *Pyrenochaeta* sp. DS3sAY3a), accompanied by high concentrations (110 to 240 μM) of Mn(III/IV). Since $MnCO_3$ is the only Mn source in these systems, the produced Mn(III/IV) must be from the fungal oxidation of Mn(II) originating from the rhodochrosite, either via direct oxidation of mineral-hosted Mn(II) or oxidation of aqueous Mn(II) provided by enhanced dissolution of $MnCO_3$. Either way, the amount of 'released Mn' as dissolved Mn(II) and oxidized Mn as Mn(III/IV) accounts for 9–25% of the total initial Mn (as $MnCO_3$), as compared with ~7% in the control sample, illustrating enhanced mineral dissolution in the presence of all fungal species.

Microscopic interrogation of the fungal–$MnCO_3$ surface points to enhanced rhodochrosite dissolution via fungal activity, likely of both chemical and physical nature

**Table 1.** Mn(III/IV) oxide location, morphology and structure derived from linear combination fitting (LCF) results for six fungal species.

| | | | LCF components and parameters | | | | |
|---|---|---|---|---|---|---|---|
| ID | Species name | Mn(III/IV) oxide location and morphology | $Mn^{2+}_{(aq)}$ | $MnCO_3$ | δ-$MnO_2$ | R factor | $\chi^2$ |
| A | *Phoma* sp. DS1wsM30b | Spherical, discrete precipitates along hyphae | 0.06 | 0.48 | 0.45 | 0.06 | 0.25 |
| B | *Pleosporales* sp. AP3s5JAC2b | Continuous coating along hyphae | 0.14 | 0.5 | 0.36 | 0.18 | 0.69 |
| C | *Pithomyces chartarum* DS1bioJ1b | Spherical, discrete precipitates along hyphae and on $MnCO_3$ surface | 0.09 | 0.79 | 0.12 | 0.12 | 0.37 |
| D | *Phoma* sp. AP3s5J1a | Continuous coating along hyphae and on $MnCO_3$ surface | 0.15 | 0.31 | 0.54 | 0.03 | 0.14 |
| E | *Pyrenochaeta* sp. DS3sAY3a | Flower-shaped oxide clusters on $MnCO_3$, sometimes underneath hyphae | 0.06 | 0.46 | 0.48 | 0.06 | 0.28 |
| F | *Stagonospora* sp. SRC1lsM3a | Flower-shaped oxide clusters on $MnCO_3$, no hyphal association | 0.09 | 0.53 | 0.37 | 0.14 | 0.48 |

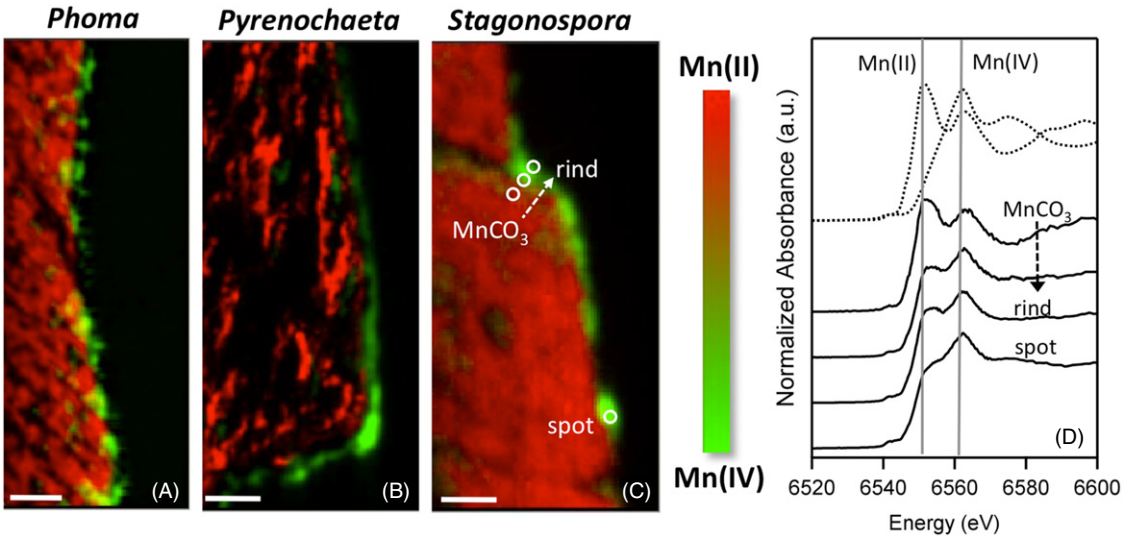


**Fig. 2.** Energy-specific synchrotron μ-X-ray fluorescence (μ-XRF) maps showing Mn(II) (red) and Mn(IV) (green) distribution in cross-thin sections of rhodochrosite reacted with (A) *Phoma* sp. DS1wsM30b, (B) *Pyrenochaeta* sp. DS3sAY3a and (C) *Stagonospora* sp. SRC1lsM3a. Scale bar represents 10 μm. (D) μ-XANES spectra taken at the white-circled areas in C (black lines), including a transect from bulk $MnCO_3$ to the Mn oxide rind and a Mn oxide hot spot. Also shown are the spectra of Mn(II) and Mn(IV) reference compounds ($MnCO_3$ and δ-$MnO_2$ respectively; dotted lines) and their peak positions (gray lines).

(Fig. S1). In the control sample (rhodochrosite without fungal inoculation), the surface after reaction with AY medium shows edge steps and isolated dissolution pits, but is otherwise smooth at the micrometre scale (Fig. S1A). Rhodochrosite crystals reacted with fungi show isolated deep dissolution pits as well as high degrees of surface etching (Fig. S1B–D). Further, hyphae were frequently observed growing into cracks and dissolution pits, suggesting a possible role for mechanical breakdown of the mineral thus increasing the surface area and reactivity of surface sites (Fig. S2). The importance of chemical and mechanical activity by fungi in mineral dissolution and alteration is widely known (Gadd, 2007). For instance, special penetrative structures (appressoria) in fungi possess high internal pressures that are believed responsible for hyphal penetration of plant tissues and rock/mineral surfaces (Howard *et al.*, 1991; Money, 1999; Bonneville *et al.*, 2009). In addition, many fungal species exude large concentrations of organic acids such as oxalic, citric, and acetic acids that are responsible for increased mineral dissolution or precipitation of secondary mineral phases (Jongmans *et al.*, 1997; Gadd, 1999; Sterflinger, 2000). In fact, high oxalate production by *Aspergillus niger* and *Serpula himantioides* has been shown to induce the dissolution and conversion of both rhodochrosite and Mn oxides to Mn oxalate minerals (Sayer *et al.*, 1997; Wei *et al.*, 2012). Here, we did not observe Mn oxalate formation via microscopic and spectroscopic analysis, likely due to the low Mn(II) levels maintained here as a result of rapid Mn(II) oxidation to Mn(III/IV).

Extensive organic surface coatings are also observed on the fungal-reacted rhodochrosite surfaces, likely contributing to mineral dissolution. For instance, on the rhodochrosite surface reacted with *Pithomyces chartarum* DS1bioJ1b (Fig. S3A and B) and *Pleosporales* sp. AP3s5JAC2b (Fig. S3C), a thin homogenous film is present consisting of a fibrous network identified at higher resolution (Fig. S3B and C). In some cases, the entire mineral surface is coated with an organic-based film, which is sometimes observed peeling away from the surface, likely a consequence of biofilm dessication during sample preparation and analysis (Fig. S3A). Based on energy dispersive X-ray (EDX) analysis, the films are not Mn oxides and instead are composed of dominantly carbon, thus likely representing an organic matrix exuded by the fungi during growth. Fungal biofilms, which are composed of a heterogeneous mixture of extracellular polymeric substances (EPS), have been implicated in bioweathering of a variety of synthetic and natural structures, including a wide range of rocks and minerals (see Gorbushina *et al.*, 2007 and references therein). Thus, the organic matrix observed here may exert an additional physical and chemical force on $MnCO_3$ weathering.

### *Distribution and speciation of oxidized* Mn *on rhodochrosite*

Synchrotron-based micro-X-ray fluorescence (μ-XRF) of thin sections of rhodochrosite reacted with three fungal species (*Phoma* sp. DS1wsM30b, *Pyrenochaeta* sp. DS3sAY3a and *Stagonospora* sp. SRC1lsM3a) illustrated

a coating of oxidized Mn, primarily as Mn(IV), on the rhodochrosite surface (Fig. 2A–C). XRF maps were collected at several incident energies around the Mn K-edge, which revealed a transition from Mn(II) within the mineral to Mn(IV) at the surface. In a section of $MnCO_3$ reacted with *Stagonospora* sp. SRC1lsM3a, μ-X-ray absorption near edge structure (μ-XANES) ($2 \times 2$ μm resolution) spectra were collected at a Mn(IV) hot spot and along a transect traversing the bulk $MnCO_3$ and surface oxide rind confirming the energy-specific μ-XRF maps (Fig. 2C and D). The bulk $MnCO_3$ spectra is nearly identical to that of the Mn(II) reference compound $MnCO_3$, with a prominent peak at ~ 6552 eV and a shoulder at ~ 6563 eV. This shoulder, although at a similar position as the Mn(IV) peak of the Mn(IV) reference spectra, is an inherent feature of the $MnCO_3$ structure. Moving outward from the bulk $MnCO_3$ to the surface rind, the main Mn(II) peak at ~ 6551 eV decreases in height, while the Mn(IV) peak at ~ 6563 eV increases, indicating an increased ratio of Mn(IV) to Mn(II) species from the bulk mineral to the oxide rind. The spectrum at the Mn(IV) hot spot (labelled 'spot') exhibits a dominant Mn(IV) peak at ~ 6563 eV and a small Mn(II) shoulder at ~ 6552 eV, indicating that the majority of Mn is present as Mn(IV) at this location. The Mn(II) signal is likely a consequence of Mn(II) incorporation within the Mn oxide structure as observed previously both for bacteria (Bargar *et al*., 2005; Webb *et al*., 2005) and for fungi grown on agar-solidified media (Santelli *et al*., 2011). Similar XANES results were also observed for rhodochrosite crystals reacted with *Phoma* sp. DS1wsM30b and *Pyrenochaeta* sp. DS3sAY3a (data not shown).

The oxidized Mn produced by all the fungal species exists as Mn oxides within the birnessite group. Principal component analysis (PCA) and linear combination fitting (LCF) of the Mn K-edge EXAFS (extended X-ray absorption fine structure) spectra for each can be reconstructed with two dominant mineral components consisting of $MnCO_3$ and δ-$MnO_2$ (Fig. S2, Table 1). δ-$MnO_2$ is a synthetic phase similar to naturally occurring vernadite, which is a poorly ordered, nanocrystalline phyllomanganate with hexagonal symmetry. In many cases, the Mn oxide products were firmly attached to the rhodochrosite surface, thus during Mn oxide harvesting for EXAFS analysis residual $MnCO_3$ particles were collected with the Mn oxide products. Addition of a minor aqueous $Mn^{2+}$ component increased the goodness of fit (Table 1). The Mn oxides formed by all six fungi grown on rhodochrosite here are similar to the frequently observed biogenic Mn oxides formed by both bacteria (Villalobos *et al*., 2003; Bargar *et al*., 2005; Webb *et al*., 2005; Learman *et al*., 2011b) and fungi (Miyata *et al*., 2006a,b; Grangeon *et al*., 2010; Santelli *et al*., 2011) under a variety of growth and environmental conditions, including the same species grown on agar-solidified media (Santelli *et al*., 2011).

### *Distribution of fungal* Mn *oxides*

Although the Mn oxide structures did not vary among the fungal species, the distribution of Mn(III/IV) oxides varied considerably and can be summarized as: (i) associated with hyphal surfaces, (ii) precipitated on the rhodochrosite surface or (iii) a combination of the two (Fig. 3, Table 1). Rhodochrosite crystals in the absence of active fungi are pink and transparent under light microscopy (not shown). Upon reaction with the six fungal species, the crystals are gradually covered with mycelia growing radially outward from the inoculation point and extending into the media-submerged quartz sand. The fungal hyphae are colourless, whereas the precipitated fungal Mn(III/IV) oxides are brown/dark brown in colour.

Two of the six species, *Phoma* sp. DS1wsM30b and *Pleosporales* sp. AP3s5JAC2b, accumulated Mn oxides along the length of their hyphae (A and B in Fig. 3 respectively). Scanning electron microscopy (SEM) images show that *Phoma* sp. DS1wsM30b produces spherical shaped Mn oxides whereas the Mn oxides formed by *Pleosporales* sp. AP3s5JAC2b uniformly coat the hyphae, over time encrusting the full length of hyphae (B in Fig. 3).

*Pithomyces chartarum* DS1bioJ1b and *Phoma* sp. AP3s5J1a also accumulated Mn oxides on the hyphal surface but a substantial amount of Mn oxides were also found on the $MnCO_3$ surface adjacent to the hyphae (C and D in Fig. 3). *Pithomyces chartarum* DS1bioJ1b produced small clusters of spherical shaped Mn oxides (C in Fig. 3), while *Phoma* sp. AP3s5J1a produced Mn oxides that encrust the hyphae (D in Fig. 3), similar to *Pleosporales* sp. AP3s5JAC2b (B in Fig. 3) but with a denser appearance.

Interestingly, two species (*Pyrenochaeta* sp. DS3sAY3a and *Stagonospora* sp. SRC1lsM3a) produced discrete, isolated flower-shaped Mn oxide clusters on $MnCO_3$ (E and F in Fig. 3) that were typically not associated with any cellular structure. Mn oxides produced by *Pyrenochaeta* sp. DS3sAY3a (E in Fig. 3) always spread laterally (20 to 100 μm in diameter) on the $MnCO_3$ surface, sometimes underneath hyphae. Oxides produced by *Stagonospora* sp. SRC1lsM3a appeared as flower-shaped clusters that are more structured three-dimensionally (F in Fig. 3) than those produced by *Pyrenochaeta* sp. DS3sAY3a. Further, the distance between the Mn oxides and hyphae at times approached 100 μm – a substantial distance away from any visible cellular structure. Intact, undisturbed hyphae were observed on the $MnCO_3$ surface, indicating that the lack of association of hyphae and Mn oxides was not an artefact of the preparation procedure.

The striking difference in the morphology and location of Mn oxides formed by different species likely points to different Mn(II) oxidation pathways or precipitation mechanisms, including but not limited to direct

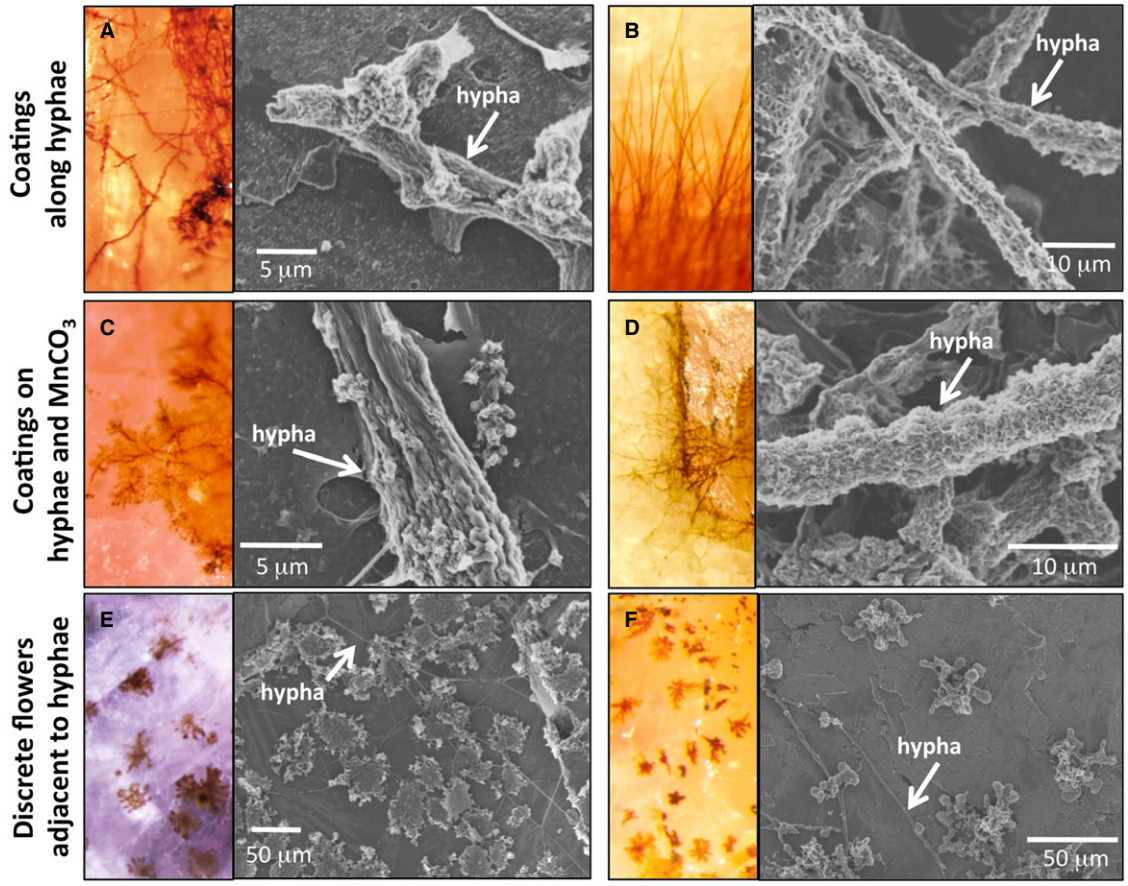


**Fig. 3.** Light and electron microscopy images showing the morphology and location of Mn oxides on rhodochrosite reacted with six fungal species (A–F; see Table 1 for species name). The brown/black colour in light microscope images represents precipitated fungal Mn(III/IV) oxides.

enzymatic oxidation, metabolite (e.g. $O_2^-$)-mediated oxidation, and/or organic-mediated complexation and/or precipitation. For example, the production of Mn oxide coatings on hyphal surfaces (e.g. B in Fig. 3) likely involves cell wall-associated enzymes (e.g. laccase-like multicopper oxidases as found in *Acremonium strictum* strain KR21-2) (Miyata *et al*., 2004; 2006a). On the contrary, the production of extracellular Mn oxide clusters that are not associated with cellular structures (e.g. E and F in Fig. 3) may point to either a metabolite-induced oxidation or a surface-associated oxidation to Mn(III) followed by complexation, transport away from the cell and ultimate precipitation at a distance. We have previously observed a similar species-based variability in Mn oxide distributions on agar-solidified media, which included Mn oxide formation by *Stagonospora* sp. SRC1lsM3a on envisaged organic polymers adjacent to hyphae (Santelli *et al*., 2011). A striking finding with this current study and not noticed previously, however, is the presence of completely isolated Mn oxides precipitated on the $MnCO_3$ surface at substantial distances from cellular structures. We focus the remaining discussion on *Pyrenochaeta* sp. DS3sAY3a and *Stagonospora* sp. SRC1lsM3a to identify a plausible pathway for Mn oxide accumulation in the absence of cellular structures.

### *Mechanisms of* Mn*(II) oxidation*

The oxidation of Mn(II) by *Pyrenochaeta* sp. DS3sAY3a and *Stagonospora* sp. SRC1lsM3a is a cell-associated process and not a result of soluble extracellular proteins or stable metabolites. Cell-free filtrate (i.e. spent media) from both organisms, obtained for cells grown both in AY liquid and on AY media-saturated quartz sand, did not oxidize either aqueous Mn(II) or Mn(II) hosted in rhodochrosite (data not shown). Thus, Mn oxide formation required the presence of actively growing hyphal cells, likely due to either cell-associated enzymes or short-lived reactive metabolites. These results are in contrast to recent findings of superoxide-mediated oxidation of Mn(II) by bacteria where the proteins involved in superoxide production were present and active in cell-free filtrate, suggesting the involvement of soluble enzyme(s) in that case (Learman *et al*., 2011a).

Incubation of fungal cultures with ROS-specific stains and various amendments to the AY growth medium implicate extracellular superoxide as the oxidant of Mn(II) by *Pyrenochaeta* sp. DS3sAY3a and *Stagonospora* sp. SRC1lsM3a (Fig. 4). Yellow, water-soluble nitroblue tetrazolium (NBT) is reduced by superoxide to form blue, water-insoluble formazan. Since the stain precipitates upon reaction with superoxide, the location of the stain precipitates reveals the site of reaction with the superoxide. Both actively growing organisms stain positively for the production of $O_2^-$ (appearance of a blue colour when incubated with NBT; Fig. 4A and B). Superoxide production is localized primarily at the hyphal tips of the leading growth edge (Fig. 4C), areas known for high metabolic activity and active cell construction.

Furthermore, Mn(II) oxidation showed a concentration-dependent inhibition by Cu(II). At the highest concentration (200 μM), Mn oxide precipitation is strongly inhibited for both *Pyrenochaeta* and *Stagonospora* (Fig. 5C and G respectively), whereas the addition of the same concentration of Zn(II) does not appreciably affect Mn oxidation (Fig. 5D and H). Cu(II) catalyses the dismutation of $O_2^-$ into $O_2$ and $H_2O_2$ (Zafiriou *et al*., 1998) and is a more effective scavenger of $O_2^-$ than Mn(II), thereby diverting fungal produced extracellular superoxide away from Mn(II) in the media. Zn(II) is used as a control, since this metal imparts a similar level of toxicity to the organisms as Cu(II) but does not interact with $O_2^-$. Although 200 μM Cu and Zn each imparts a slight reduction in growth rate of the fungal mycelium in both organisms (e.g. compare Fig. 5C and G with A and E respectively), the impacts of the two metals are similar and do not confound the implication of $O_2^-$ in Mn(II) oxidation. Taken together with the observations of superoxide formation at hyphal tips, these findings implicate superoxide as the oxidant of Mn(II) by both fungal species. The primary enzymes responsible for superoxide production in fungi are NADPH oxidases within the NOX family (Aguirre *et al*., 2005; Scott and Eaton, 2008).

Indeed, superoxide production and subsequent Mn(II) oxidation is linked to the activity of NADPH oxidases in both *Pyrenochaeta* sp. DS3sAY3a and *Stagonospora* sp. SRC1lsM3a. Mn oxide precipitation is substantially decreased in the presence of 25 μM (Fig. 5B) and 10 μM (Fig. 5F) diphenylene iodonium (DPI) chloride, an inhibitor of oxidoreductases and other NAD(P)H binding enzymes known to produce superoxide in fungi (O'Donnell *et al*., 1993). This superoxide is involved in host defence, post-translational modification of proteins, apical growth and branching of hyphae, cell signalling and cell differentiation (Aguirre *et al*., 2005). Here, in addition to Mn(II) oxidation inhibition, the addition of DPI leads to a decrease in fungal growth, particularly for *Stagonospora* sp. SRClsM3a, likely due to disruption of hyphal growth. NOX proteins in fungi are transmembrane proteins that transport electrons from cytosolic NADPH via FAD and two haems to extracellular molecular oxygen to generate $O_2^-$. This localization is consistent with the lack of Mn(II) oxidation activity in cell-free extracts, whereby the production of superoxide occurs at the cell surface leading to reaction between superoxide and Mn(II) near the hyphal surface. These results are similar to recent findings that the Ascomycete *Stilbella aciculosa* (Hansel *et al*., 2012) oxidizes Mn(II) via superoxide production during asexual reproduction, suggesting that this ROS-mediated Mn(II) oxidation mechanism may be common among Ascomycetes.

Interestingly, in both *Pyrenochaeta* sp. DS3sAY3a and *Stagonospora* sp. SRC1lsM3a, small, spherical Mn

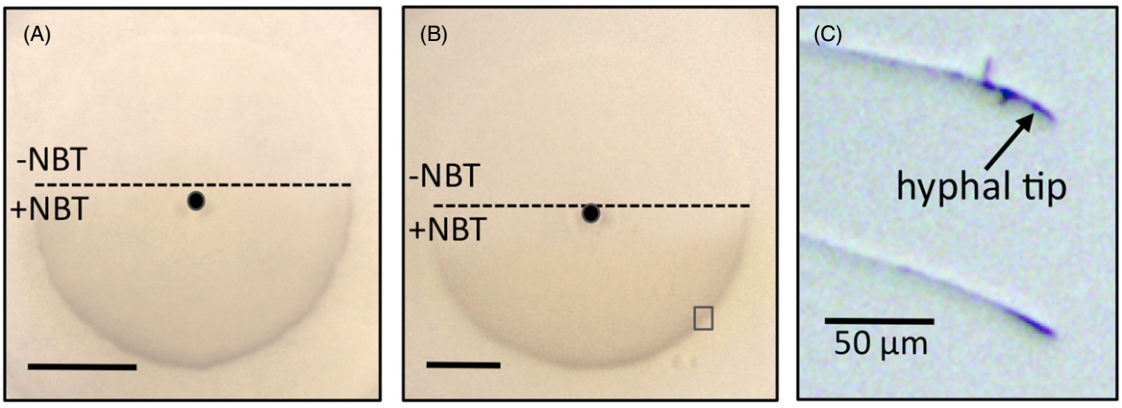


**Fig. 4.** Distribution of superoxide for *Pyrenochaeta* sp. DS3sAY3a (A) and *Stagonospora* sp. SRC1lsM3a (B and C). Images show circular fungal mycelia on AY agar plates after approximately 2 weeks of growth starting from a centre inoculation point (indicated by a black dot).
A and B. Lower portions of mycelia (below dotted lines) were stained with NBT. Blue colour indicates the presence of $O_2^-$. Cells were grown without added Mn(II). Scale bars are 1 cm.
C. Higher magnification image of the leading hyphal edge of *Stagonospora* sp. SRC1lsM3a (as indicated in boxed region in B) indicating the distribution of superoxide at the hyphal tip. Scale bar = 50 μm.

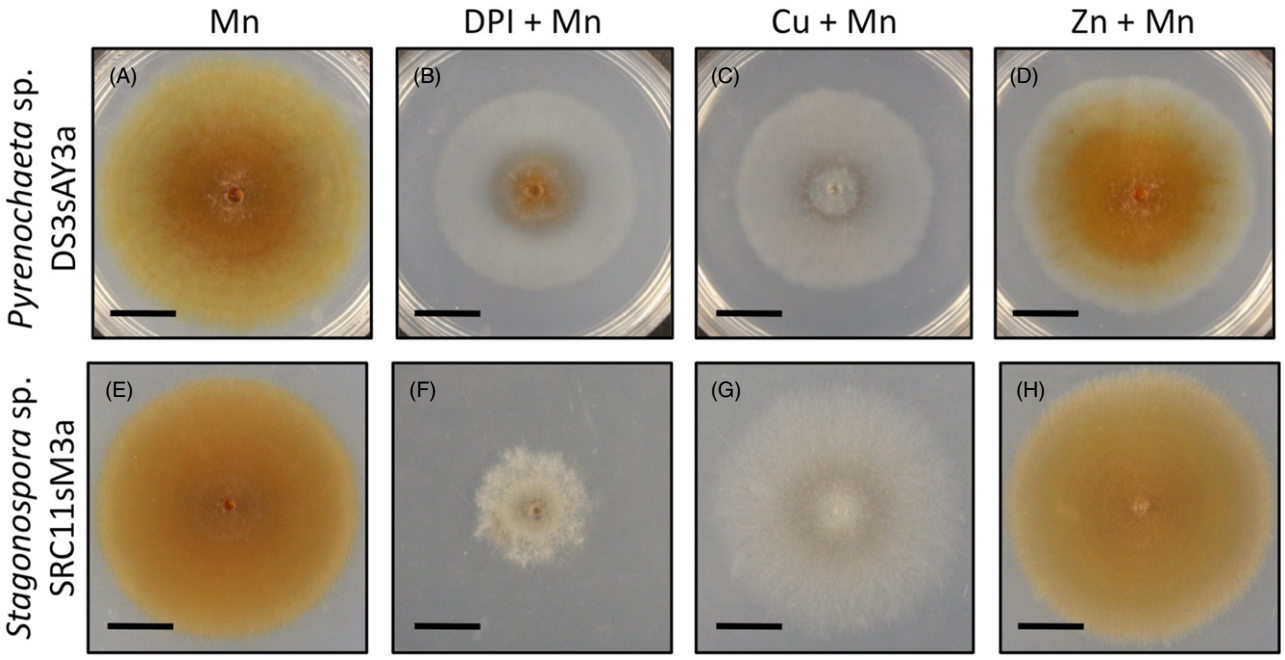


**Fig. 5.** Impact of chemical/enzyme inhibitors on Mn oxide formation by *Pyrenochaeta* sp. DS3sAY3a (A–D) and *Stagonospora* sp. SRC1lsM3a (E–H).
A and E. AY agar controls amended with 200 μM Mn(II). Brown colour indicates mycogenic Mn oxides.
B and F. Cells grown with 200 μM Mn(II) and 25 μM (B) or 10 μM (F) DPI, an inhibitor of NADPH oxidases.
C and G. Cells grown with 200 μM Mn(II) and 200 μM Cu(II), a scavenger of superoxide.
D and H. Cells grown with 200 μM Mn(II) and 200 μM Zn(II). Zn(II) imparts a similar level of toxicity as Cu(II) but does not react with superoxide.
All scale bars are 1 cm.

oxides (confirmed via addition of LBB) were produced at a distance from fungal hyphae in the presence of high Cu(II) levels (Fig. S5C and G) and DPI (Fig. S5B and F). It is unclear at this time the mechanism of Mn(II) oxidation responsible for these structures, but considering they are observed only in the presence of high Cu and DPI, this may be a consequence of a stress response.

Taken together, the primary mechanism of Mn(II) oxidation by *Pyrenochaeta* sp. DS3sAY3a and *Stagonospora* sp. SRC1lsM3a is a result of extracellular superoxide production at the hyphal surface (Figs 4 and 5) due to the activity of transmembrane NADPH oxidases. The oxidation of Mn(II) by superoxide produces Mn(III), which is thermodynamically unstable in aqueous solutions. Yet, the Mn oxides produced by *Pyrenochaeta* sp. DS3sAY3a and *Stagonospora* sp. SRC1lsM3a show no association with hyphae and appear as discrete clusters at a substantial distance (10–100 μm) from cellular structures (Fig. 3). This suggests that either Mn(III) is being stabilized and transported away from the cell surface or superoxide is diffusing away from the hyphal tip and reacting with Mn(II) away from the cell. However, the localized precipitation of the NBT stain at hyphal tips suggests that superoxide is not diffusing far from the site of formation (Fig. 4). Instead, stabilization of Mn(III) could occur via complexation with an organic ligand and/or siderophore allowing for its transport away from the hyphae until the discrete flower-shaped Mn oxides precipitate.

### Mn *oxides formed following superoxide-mediated* Mn*(II) oxidation*

The Mn oxides produced by *Pyrenochaeta* sp. DS3sAY3a and *Stagonospora* sp. SRC1lsM3a are unique in character and illustrate an intriguing ordered morphology (Fig. 6) suggesting that mineral growth was directed by an unknown organic template. Although the oxides produced by *Pyrenochaeta* sp. DS3sAY3a were more spread out laterally (Fig. 6A) and those produced by *Stagonospora* sp. SRC1lsM3a were more structured three-dimensionally (Fig. 6D), close examination of both fungal Mn oxides revealed similar densely packed threads of oxides that were tens to hundreds of nanometres in diameter and a few microns in length (Fig. 6B, C, E and F). Some aggregated fibres observed for *Stagonospora* sp. SRC1lsM3a had a round feature at the end (Figs 6F and 7), which to our knowledge is a morphology unique to this organism. The interesting morphology of Mn oxides produced by these two species is similar to previously reported *Metallogenium*-like structures (Klaveness, 1977; Emerson

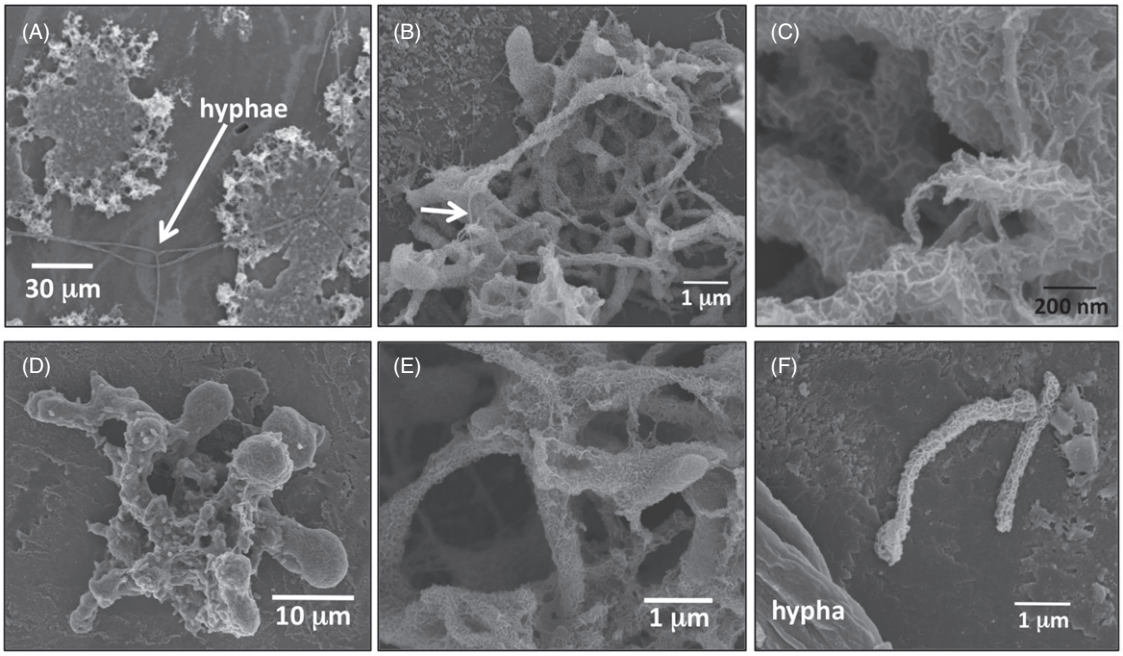


**Fig. 6.** SEM images of the Mn oxides formed by (A–C) *Pyrenochaeta* sp. DS3sAY3a and (D–F) *Stagonospora* sp. SRC1lsM3a grown on rhodochrosite. Images illustrate structurally unique Mn oxides with visible unknown filaments (see arrow in B) within the oxides. Hyphae are not in the field of view for images B–E.

*et al*., 1989). Such structures have been observed in a variety of modern and ancient aquatic and terrestrial environments (Perfil'ev and Gabe, 1961; Crerar *et al*., 1980; Gregory *et al*., 1980; Dubinina, 1984; Neretin *et al*., 2003). *Metallogenium* was originally described as a genus of bacteria that is capable of oxidizing Mn(II) (Perfil'ev and Gabe, 1961). However, a later study (Emerson *et al*., 1989) revealed that these filamentous Mn oxides were not templated on any cellular structure (bacterial or fungal) and were instead precipitated on a matrix of anionic polymers, likely consisting of acidic polysaccharides and/or proteins.

Indeed, similar to *Metallogenium*-like structures, high-resolution transmission electron microscopy (TEM) imaging of the Mn oxides did not reveal any observable cellular structures associated with the Mn oxides (Fig. 7). We have shown previously that the Mn oxides formed by *Stagonospora* sp. on Mn(II)-supplemented agar-solidified medium and in liquid culture appeared as dense masses of Mn oxides composed of filaments not templated on any visible cellular structure (Santelli *et al*., 2011). Both TEM imaging of whole mounts (Fig. 7A–C) and high-resolution imaging of thin sections (Fig. 7D) do not reveal any visible cellular structure within the Mn oxides. Instead, the Mn oxides appear highly ordered with radial growth along what appears to be a directed growth front. In fact, thin unidentified filaments are observed emerging from the Mn oxides precipitated on $MnCO_3$ (see arrow in Fig. 6B) that are not Mn oxides and are too thin to be fungal hyphae. These filaments may in fact be involved in the directed growth. Similarly, organic-directed growth has been proposed for Mn and Fe oxide encrustations on the surfaces of budding and sheathed bacteria (Ghiorse, 1984) and bacterial stalks (Chan *et al*., 2004; 2009). In fact, our preliminary micro-Fourier transform infrared spectroscopy (μ-FTIR) analysis of Mn oxides reveals the presence of various organic functional groups (e.g. amide I and II groups) (Fig. S6), hinting at the presence of proteins templates. We are actively investigating the mechanisms of Mn(III) transport and Mn oxide formation, including the role of organic templates, by *Pyrenochaeta* sp. DS3sAY3a and *Stagonospora* sp. SRC1lsM3a.

In this study, we show that fungi can be agents of rhodochrosite dissolution and conversion to Mn oxides, minerals of substantial relevance in metal and nutrient availability and transport. Rhodochrosite dissolution was substantially enhanced in the presence of fungi. In particular, the activity of some fungi released/oxidized up to 25% of the mineral-hosted Mn(II) within 22 days. Fungal activity could therefore be a dominant process for rhodochrosite dissolution within sediments and soils. Despite the similarity in the structures of the Mn oxides produced by six fungal species, we show that the morphology of the oxides produced and the location relative to the fungal and mineral surface vary among species. As suggested previously for agar-supported fungal growth (Santelli *et al*., 2011), these differences likely point to more than one operative Mn(II) oxidation pathway employed by fungi. The formation of Mn oxides at substantial distances

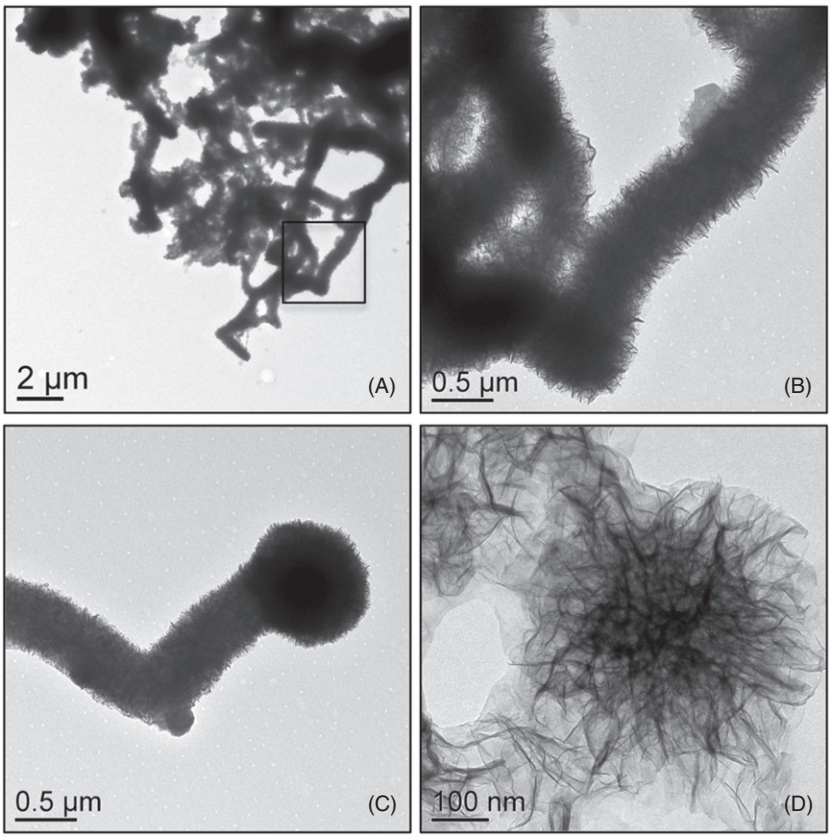


**Fig. 7.** TEM images of whole mounts (A–C) and cross section (D) of Mn oxides produced by *Stagonospora* sp. SRC1lsM3a grown in liquid AY medium.
A. An aggregate of extracellular, thread-like Mn oxides.
B. Magnified view of boxed area in A.
C. An individual thread-like Mn oxide filament with a ball-like feature at the tip.
D. Cross section of a ball-like feature (modified from Santelli *et al.*, 2011).

away from the hyphae of *Pyrenochaeta* sp. DS3sAY3a and *Stagonospora* sp. SRC1lsM3a is attributed to Mn(II) oxidation by extracellular superoxide at the hyphal surface likely followed by Mn(III) complexation and ultimately heterogeneous precipitation. Thus, these findings expand the group of organisms that oxidize Mn(II) by producing superoxide (Learman *et al.*, 2011a; Hansel *et al.*, 2012), where here it is likely a result of cell differentiation. The unique morphology of the isolated flower-like Mn oxide clusters and presence of organic functional groups associated with these oxides suggests a role of mycogenic organic polymers in Mn oxide templation. Further investigations are underway to define the role and composition of organic molecules (likely protein) in directed precipitation. These findings highlight the diversity of fungi–Mn oxide relationships and processes responsible for fungal Mn oxide precipitation. Building off this foundation, this research will shed light on environmental Mn oxide formation, including the frequently observed *Metallogenium*-like Mn oxide structures.

## Experimental procedures

### *Fungal species and growth conditions*

We explored a total of six Mn(II)-oxidizing ascomycetes isolated from two locations. Four species were isolated from passive coal mine drainage treatment systems in Central Pennsylvania that attenuate high concentrations of Mn (Santelli *et al.*, 2010): *Stagonospora* sp. SRC1lsM3a, *Phoma* sp. DS1swM30b, *Pyrenochaeta* sp. DS3sAY3a and *Pithomyces chartarum* DS1bioJ1b (Santelli *et al.*, 2010). Two species were isolated from Ashumet Pond, MA, a natural freshwater lake: *Phoma* sp. AP3s5J1a and *Pleosporales* sp. AP3s5JAC2b (C.M. Santelli, unpubl. data). This field site was previously contaminated with a sewage plume from Massachusetts Military Reservation (MMR) containing elevated concentrations of phosphorus and other constituents such as manganese.

$MnCO_3$ (sample # 96030, Colorado) was obtained from the Harvard University Mineralogical Museum. Fresh flat surfaces (mm in size) were prepared by cleaving large crystals with a razor blade along the $\{10\bar{1}4\}$ plane and sterilized by autoclaving at 121°C for 15 min.

All fungal species were grown in HEPES-buffered (20 mM, pH 7) AY medium composed of 0.25 g $l^{-1}$ sodium acetate, 0.15 g $l^{-1}$ yeast extract and 1 ml $l^{-1}$ trace element stock (10 mg $l^{-1}$ $CuSO_4{\cdot}5H_2O$, 44 mg $l^{-1}$ $ZnSO_4{\cdot}7H_2O$, 20 mg $l^{-1}$ $CoCl_2{\cdot}6H_2O$ and 13 mg $l^{-1}$ $Na_2MoO_4{\cdot}2H_2O$) supplemented with $MnCl_2$ (0–200 µM), $CuCl_2$ (0–200 µM), $ZnCl_2$ (0–200 µM) and/or DPI (0–50 µM). Fungal cultures were first initiated in Petri dishes containing agar-solidified (2% agar) AY medium without supplements. After growth proceeded radially outward from the inoculation point for approximately 2 weeks, the fungal mycelia were sampled with either a sterile coring device (for rhodochrosite cultures) or a sterile wooden inoculation stick (for plate cultures).

For cultures grown on rhodochrosite, a Petri dish containing 3–5 ml of liquid AY medium [without any additional sources of Mn(II)] was filled with sterile quartz sand to maintain moisture and provide a solid support for the rhodochrosite crystals. Several crystals were gently placed on the sand. Mycelia-containing agar plugs obtained with the sterile coring device were then placed on the rhodochrosite surfaces. Cultures were incubated for 2–3 weeks at room temperature. Growth of fungal mycelia and production of dark brown Mn oxides were monitored with a light microscope (as described below). The formation of Mn(III, IV) oxides was confirmed with the LBB method (Krumbein and Altmann, 1973) using a Cary 50 UV-vis spectrophotometer (Varian).

To compare the relative efficiency of Mn oxide production from rhodochrosite among the six fungal species, a separate set of experiments was conducted. For each species, a Petri dish containing 3 ml of AY medium [without Mn(II) or other supplements] and 258 ± 48 mg of rhodochrosite was inoculated with a mycelia-containing agar plug. Care was taken to ensure that all agar plugs were of similar size. Triplicates were conducted for each species. After 22 days, production of dark brown Mn oxides was examined for all species. From each Petri dish, 0.25 ml of the spent media was syringe filtered (0.2 μm PTFE membrane), and Mn(II) concentration was analysed using the formaldoxime method (Goto *et al*., 1962). The rest of the solution and all reacted crystals were sacrificed and analysed for Mn(III, IV) oxide concentration using the LBB method.

For plate cultures, new AY agar plates (with or without supplements) were inoculated with wooden inoculation sticks and allowed to grow for 2–3 weeks, at which point ROS detection assays and/or imaging with a stereo microscope were performed (described below). All cultures were incubated at room temperature.

### *Reactive oxygen species detection*

Extracellular ROS were detected using stains that precipitate upon reaction with ROS, thus maintaining spatial distribution of ROS production on agar-solidified media. Cultures grown on AY plates were point inoculated with NBT or DAB for superoxide and hydrogen peroxide detection, respectively. The NBT assay involved addition of 2.5 mM NBT chloride (Sigma, St Louis, MO, USA) in 5 mM 3-(*N*-morpholino)propanesulfonate-NaOH, pH 7.6, which forms a blue precipitate upon reaction with $O_2^-$. The DAB assay involved addition of 2.5 mM DAB and 5 purpurogallin units $ml^{-1}$ of horseradish peroxidase (HRP) in potassium phosphate buffer, pH 6.9, which forms a reddish brown precipitate upon reaction with $H_2O_2$, a dismutation product of the highly reactive superoxide radical. All reagents for the DAB assay were obtained from a HRP chromogen kit (GeneTex, Irvine, CA, USA). For both assays, plates were incubated with the stain for 30 min in the dark. Then, excess reagents were decanted, and the plates were incubated for an additional 2–24 h until sufficient colour had developed. The plates were imaged using a stereo microscope (as described below).

### *Light and electron microscopy*

Light microscopy images of pristine and fungal-reacted rhodochrosite crystals and agar-supported plate cultures were recorded at various time stages using a SZX16 Zoom Stereo Microscope (Olympus America) fitted with an Olympus DP72 Microscope Digital Camera.

For SEM, rhodochrosite crystals covered with fungal mycelia and Mn oxides were fixed in 2.5% glutaraldehyde, washed three times in 0.2 M phosphate buffer (pH 7.4) and subjected to a series of ethanol dehydration. After the fixation process, desiccated samples were mounted on double-sided carbon tape and sputter-coated with Pt/Pd prior to imaging. SEM was performed at the Harvard University Center for Nanoscale Systems (CNS) using field emission SEMs (FESEM; Zeiss Ultra55 and Supra55) with a high-efficiency in-lens secondary electron detector.

For TEM, dehydrated cultures that were grown in liquid media were embedded in LR White resin and cured at 60°C overnight. Hardened resin blocks were sectioned to 70 nm with a Diatome 45° diamond knife using a Leica UCT ultramicrotome (Leica Microsystems). Both unembedded dehydrated cultures and embedded sections were mounted on 100 mesh copper grids with formvar support film coated with carbon. Unstained sections were imaged with an FEI Tecnai T-12 cryo-TEM. Thin sections were examined using a JEOL 2010 high-resolution TEM (HR-TEM) equipped with an Oxford ISIS energy-dispersive X-ray spectroscopy (EDS) microanalysis system.

### *Synchrotron-based microscopic and spectroscopic analysis*

Rhodochrosite crystals reacted with *Phoma* sp. DS1wsM30b, *Pyrenochaeta* sp. DS3sAY3a and *Stagonospora* sp. SRC1lsM3a were examined by coupled synchrotron-based micro-X-ray fluorescence (μ-XRF) microscopy and micro-X-ray absorption spectroscopy (μ-XAS) at beamline 2–3 at the Stanford Synchrotron Radiation Lightsource (SSRL) for the location and oxidation state of the associated Mn. Reacted crystals were air dried and embedded in EpoHeat Epoxy (Buehler). Cross sections (~ 100 μm thickness) of the embedded crystals were obtained using a diamond saw, fixed to a high-purity quartz slide using Hillquist Thin Section Epoxy A-B (Hillquist) and polished to ~ 50 μm thickness. Spatially resolved (micron scale) XRF and XAS were conducted by collecting spectra at select points of interest or rastering a defined region. The beam size on the sample was 2 × 2 μm. Monochromatic X-rays were selected using a Si(111) $\Phi = 90$ double crystal monochromator. Multiple elements were mapped simultaneously by collecting fluorescence on a multichannel Si Vortex detector (SII Nano Technology) using an incident monochromator energy of 13 200 eV which is above the absorption edge of all the elements of interest. Maps were also collected at several discrete incident energies (6553, 6558, 6562 eV) in continuous raster scanning mode in order to collect the fluorescence at several distinguishing points within the Mn absorption edge. X-ray absorption near edge structure spectra were collected at spots of interest to confirm the oxidation state at discrete locations. The line shapes (peak position and peak shape) of the XANES spectra were used to compare the relative proportions of Mn(II), Mn(III) and

Mn(IV) in the Mn oxides (Bargar *et al*., 2005; Webb *et al*., 2005). Fluorescence maps and XANES spectra were analysed using the MicroAnalysis Toolkit (Webb, 2006) and SIXPACK (Webb, 2005) respectively.

Bulk X-ray absorption spectroscopy data were also collected on the fungal Mn oxides to identify their speciation and structure. For all six species, mycogenic Mn oxides from reacted rhodochrosite were carefully separated by hand picking with tweezers under a microscope or brief ultrasonication in DI water. The collected Mn oxides were vacuum filtered using 0.2 μm polycarbonate membranes and rinsed with DI water. Multiple crystals were processed to achieve enough mass. The moist filter membranes loaded with Mn oxides were then mounted in a Teflon sample holder covered with Kapton tape for XAS data analysis. Samples were frozen at –20°C and thawed prior to analysis. Manganese K-edge XAS spectra were collected at beam line 11-2 (SSRL) and beam line X18B at National Synchrotron Light Source, Brookhaven National Laboratory (NSLS-BNL) with a Si (220) or (111) double crystal monochromator (40% detuning). Energy calibration used a Mn foil (6539 eV). Data were collected in both fluorescence and transmission mode using a 30-element Ge solid-state detector with a Cr filter at beam line 11-2 (SSRL) and a PIPS detector at beam line X18B (NSLS). Analysis of the near edge region of consecutive XAS spectra for each sample showed no photo-induced reduction of Mn oxides under the X-ray beam.

Analysis of the bulk XAS data was performed using the programs SIXPACK (Webb, 2005) and Ifeffit (Ravel and Newville, 2005). The composition and structure of fungal Mn oxides were determined using both the XANES and EXAFS regions. For EXAFS analysis, spectra were $k^3$-weighted and analysed at 3–12 $Å^{-1}$. Principal component analysis (PCA), combined with target transformation and linear combination fitting (LCF), were performed on the EXAFS spectra to establish the number of components representing the entire data set. A spectral reference library of model Mn compounds was used to identify and quantify the structural components. The model compounds used were previously described (Bargar *et al*., 2005) and include: δ-$MnO_2$, hexagonal Na-birnessite, triclinic Ca-birnessite, groutite (α-MnOOH), feitknechtite (β-MnOOH), manganite (γ-MnOOH), hausmannite ($Mn_3O_4$), synthetic todorokite [$(Na,Ca,K)(Mg,Mn)Mn_6O_{14}·5H_2O$], pyrolusite (β-$MnO_2$), synthetic $Mn_2O_3$, aqueous Mn(III) pyrophosphate, aqueous $MnCl_2$ and aqueous $MnSO_4$.

## Acknowledgements

The authors thank Adiari I. Vázquez-Rodríguez for help with thin section preparation, Christopher Lentini and Emily Estes for help with EXAFS data collection, Sam Webb (SSRL) for support on beamline 2–3, and Alice Dohnalkova (EMSL) for assistance in TEM collection. The authors also thank Associate Editor Victoria Orphan and the anonymous reviewers for their helpful suggestions. Portions of this research were conducted at the Stanford Synchrotron Radiation Lightsource (SSRL), the National Synchrotron Light Source (NSLS), the Center for Nanoscale Systems (CNS) at Harvard University and the Environmental Molecular Sciences Lab (EMSL). SSRL is a national user facility operated by Stanford University on behalf of the US Department of Energy, Office of Basic Energy Sciences. The SSRL Structural Molecular Biology Program is supported by the Department of Energy, Office of Biological and Environmental Research and by the National Institutes of Health, National Center for Research Resources, Biomedical Technology Program. NSLS is supported by the US Department of Energy, Office of Science, Office of Basic Energy Sciences, under Contract No. DE-AC02-98CH10886. CNS is a member of the National Nanotechnology Infrastructure Network (NNIN), which is supported by the National Science Foundation under NSF Award No. ECS-0335765. CNS is part of the Faculty of Arts and Sciences at Harvard University. EMSL is a national scientific user facility sponsored by the Department of Energy's Office of Biological and Environmental Research located at Pacific Northwest National Laboratory. This project was funded by the National Science Foundation, Grant Number EAR-0846715, awarded to C. M. H.

## References

Aguirre, J., Rios-Momberg, M., Hewitt, D., and Hansberg, W. (2005) Reactive oxygen species and development in microbial eukaryotes. *Trends Microbiol* **13:** 111–118.

Bargar, J.R., Tebo, B.M., Bergmann, U., Webb, S.M., Glatzel, P., Chiu, V.Q., and Villalobos, M. (2005) Biotic and abiotic products of Mn(II) oxidation by spores of the marine *Bacillus* sp. strain SG-1. *Am Mineral* **90:** 143–154.

Bedard, K., Lardy, B., and Krause, K.H. (2007) NOX family NADPH oxidases: not just in mammals. *Biochimie* **89:** 1107–1112.

Bonneville, S., Smits, M.M., Brown, A., Harrington, J., Leake, J.R., Brydson, R., and Benning, L.G. (2009) Plant-driven fungal weathering: early stages of mineral alteration at the nanometer scale. *Geology* **37:** 615–618.

Cahyani, V.R., Murase, J., Ishibashi, E., Asakawa, S., and Kimura, M. (2009) Phylogenetic positions of Mn(2+)-oxidizing bacteria and fungi isolated from Mn nodules in rice field subsoils. *Biol Fertil Soils* **45:** 337–346.

Chan, C.S., De Stasio, G., Welch, S.A., Girasole, M., Frazer, B.H., Nesterova, M.V., *et al*. (2004) Microbial polysaccharides template assembly of nanocrystal fibers. *Science* **303:** 1656–1658.

Chan, C.S., Fakra, S.C., Edwards, D.C., Emerson, D., and Banfield, J.F. (2009) Iron oxyhydroxide mineralization on microbial extracellular polysaccharides. *Geochim Cosmochim Acta* **73:** 3807–3818.

Chan, C.S., Fakra, S.C., Emerson, D., Fleming, E.J., and Edwards, K.J. (2011) Lithotrophic iron-oxidizing bacteria produce organic stalks to control mineral growth: implications for biosignature formation. *ISME J* **5:** 717–727.

Chen, G.Q., Zou, Z.J., Zeng, G.M., Yan, M., Fan, J.Q., Chen, A.W., *et al*. (2011) Coarsening of extracellularly biosynthesized cadmium crystal particles induced by thioacetamide in solution. *Chemosphere* **83:** 1201–1207.

Crerar, D.A., Fisher, A.G., and Plaza, C.L. (1980) *Metallogenium* and biogenic deposition of manganese from Precambrian to recent time. In *Geology and Geochemistry of Manganese, Volume III, Manganese on the Bottom of Recent Basins*. Vanentsov, I.M., and Grasselly, G. (eds). Stuttgart, Germany: Verlagsbuchhandlung, pp. 285–303.

Diem, D., and Stumm, W. (1984) Is dissolved $Mn^{2+}$ being oxidized by $O_2$ in absence of Mn-bacteria or surface catalysts? *Geochim Cosmochim Acta* **48:** 1571–1573.

Dubinina, G.A. (1984) Infection of Procaryotic and eukaryotic microorganisms with *Metallogenium*. *Curr Microbiol* **11:** 349–356.

Emerson, D., Garen, R.E., and Ghiorse, W.C. (1989) Formation of *Metallogenium*-like structures by a manganese-oxiding fungus. *Arch Microbiol* **151:** 223–231.

Feng, X.H., Zhu, M.Q., Ginder-Vogel, M., Ni, C.Y., Parikh, S.J., and Sparks, D.L. (2010) Formation of nano-crystalline todorokite from biogenic Mn oxides. *Geochim Cosmochim Acta* **74:** 3232–3245.

Gadd, G.M. (1999) Fungal production of citric and oxalic acid: importance in metal speciation, physiology and biogeochemical processes. *Adv Microb Physiol* **41:** 47–92.

Gadd, G.M. (2007) Geomycology: biogeochemical transformations of rocks, minerals, metals and radionuclides by fungi, bioweathering and bioremediation. *Mycol Res* **111:** 3–49.

Ghiorse, W.C. (1984) Biology of iron- and manganese-depositing bacteria. *Annu Rev Microbiol* **38:** 515–550.

Ghiorse, W.C., and Hirsch, P. (1979) Ultrastructural-study of iron and manganese deposition associated with extracellular polymers of *Pedomicrobium*-like budding bacteria. *Arch Microbiol* **123:** 213–226.

Glenn, J.K., Akileswaran, L., and Gold, M.H. (1986) Mn(II) oxidation is the principal function of the extracellular Mn-peroxidase from *Phanerochaete chrysosporium*. *Arch Biochem Biophys* **251:** 688–696.

Golden, D., Zuberer, D., and Dixon, J. (1992) Manganese oxides produced by fungal oxidation of manganese from siderite and rhodochrosite. In *Biomineralization Processes of Iron and Manganese: Modern and Ancient Environments (Catena Supplement)*. Skinner, H.C.W., and Fitzpatrick, R.W. (eds). Cremlingen-Destedt, Germany: Catena Verlag, pp. 161–168.

Gorbushina, A.A., Kort, R., Schulte, A., Lazarus, D., Schnetger, B., Brumsack, H.J., *et al*. (2007) Life in Darwin's dust: intercontinental transport and survival of microbes in the nineteenth century. *Environ Microbiol* **9:** 2911–2922.

Goto, K., Komatsu, T., and Furukawa, T. (1962) Rapid colorimetric determination of manganese in waters containing iron – a modification of formaldoxime method. *Anal Chim Acta* **27:** 331–334.

Grangeon, S., Lanson, B., Miyata, N., Tani, Y., and Manceau, A. (2010) Structure of nanocrystalline phyllomanganates produced by freshwater fungi. *Am Mineral* **95:** 1608–1616.

Gregory, E., Perry, R.S., and Staley, J.T. (1980) Characterization, distribution, and significance of *Metallogenium* in Lake Washington. *Microb Ecol* **6:** 125–140.

Hansard, S.P., Easter, H.D., and Voelker, B.M. (2011) Rapid reaction of nanomolar Mn(II) with superoxide radical in seawater and simulated freshwater. *Environ Sci Technol* **45:** 2811–2817.

Hansel, C.M., and Francis, C.A. (2006) Coupled photochemical and enzymatic Mn(II) oxidation pathways of a planktonic *Roseobacter*-like bacterium. *Appl Environ Microbiol* **72:** 3543–3549.

Hansel, C.M., Zeiner, C.A., Santelli, C.M., and Webb, S.M. (2012) Mn(II) oxidation by an ascomycete fungus is linked to superoxide production during asexual reproduction. *Proc Natl Acad Sci USA* **109:** 12621–12625.

Hofer, C., and Schlosser, D. (1999) Novel enzymatic oxidation of $Mn^{2+}$ to $Mn^{3+}$ catalyzed by a fungal laccase. *FEBS Lett* **451:** 186–190.

Howard, R.J., Ferrari, M.A., Roach, D.H., and Money, N.P. (1991) Penetration of hard substrates by a fungus employing enormous turgor pressures. *Proc Natl Acad Sci USA* **88:** 11281–11284.

Jongmans, A.G., vanBreemen, N., Lundstrom, U., vanHees, P.A.W., Finlay, R.D., Srinivasan, M., *et al*. (1997) Rock-eating fungi. *Nature* **389:** 682–683.

Klaveness, D. (1977) Morphology, distribution and significance of manganese-accumulating microorganism *Metallogenium* in lakes. *Hydrobiologia* **56:** 25–33.

Klewicki, J.K., and Morgan, J.J. (1998) Kinetic behavior of Mn(III) complexes of pyrophosphate, EDTA, and citrate. *Environ Sci Technol* **32:** 2916–2922.

Klewicki, J.K., and Morgan, J.J. (1999) Dissolution of β-MnOOH particles by ligands: pyrophosphate, ethylenediaminetetraacetate, and citrate. *Geochim Cosmochim Acta* **63:** 3017–3024.

Kostka, J.E., Luther, G.W., and Nealson, K.H. (1995) Chemical and biological reduction of Mn(III)-pyrophosphate complexes – potential importance of dissolved Mn(III) as an environmental oxidant. *Geochim Cosmochim Acta* **59:** 885–894.

Krumbein, W.E., and Altmann, H.J. (1973) A new method for detection and enumeration of manganese oxidizing and reducing microorganisms. *Helgol Wiss Meeresunters* **25:** 347–356.

Lafferty, B.J., Ginder-Vogel, M., and Sparks, D.L. (2010) Arsenite oxidation by a poorly crystalline manganese-oxide 1. Stirred-flow experiments. *Environ Sci Technol* **44:** 8460–8466.

Learman, D.R., Voelker, B.M., Vazquez-Rodriguez, A.I., and Hansel, C.M. (2011a) Formation of manganese oxides by bacterially generated superoxide. *Nat Geosci* **4:** 95–98.

Learman, D.R., Wankel, S.D., Webb, S.M., Martinez, N., Madden, A.S., and Hansel, C.M. (2011b) Coupled biotic-abiotic Mn(II) oxidation pathway mediates the formation and structural evolution of biogenic Mn oxides. *Geochim Cosmochim Acta* **75:** 6048–6063.

Lenz, M., Kolvenbach, B., Gygax, B., Moes, S., and Corvini, P.F.X. (2011) Shedding light on selenium biomineralization: proteins associated with bionanominerals. *Appl Environ Microbiol* **77:** 4676–4680.

Luther, G.W. (2005) Manganese(II) oxidation and Mn(IV) reduction in the environment – two one-electron transfer steps versus a single two-electron step. *Geomicrobiol J* **22:** 195–203.

Luther, G.W. (2010) The role of one- and two-electron transfer reactions in forming thermodynamically unstable intermediates as barriers in multi-electron redox reactions. *Aquat Geochem* **16:** 395–420.

Luther, G.W., Ruppel, D.T., and Burkhard, C. (1998) Reactivity of dissolved Mn(III) complexes and Mn(IV) species with reductants: Mn redox chemistry without a dissolution step. In *ACS Symposium Series, Vol. 715, Mineral-Water Interfacial Reactions: Kinetics and Mechanisms*. Sparks,

D.L., and Grundl, T.J. (eds). Washington, DC, USA: American Chemical Society, pp. 265–280.

Miyata, N., Tani, Y., Iwahori, K., and Soma, M. (2004) Enzymatic formation of manganese oxides by an *Acremonium*-like hyphomycete fungus, strain KR21-2. *FEMS Microbiol Ecol* **47:** 101–109.

Miyata, N., Tani, Y., Maruo, K., Tsuno, H., Sakata, M., and Iwahori, K. (2006a) Manganese(IV) oxide production by *Acremonium* sp strain KR21-2 and extracellular Mn(II) oxidase activity. *Appl Environ Microbiol* **72:** 6467–6473.

Miyata, N., Maruo, K., Tani, Y., Tsuno, H., Seyama, H., Soma, M., and Iwahori, K. (2006b) Production of biogenic manganese oxides by anamorphic ascomycete fungi isolated from streambed pebbles. *Geomicrobiol J* **23:** 63–73.

Miyata, N., Tani, Y., Sakata, M., and Iwahori, K. (2007) Microbial manganese oxide formation and interaction with toxic metal ions. *J Biosci Bioeng* **104:** 1–8.

Money, N.P. (1999) Biophysics – fungus punches its way in. *Nature* **401:** 332–333.

Moreau, J.W., Weber, P.K., Martin, M.C., Gilbert, B., Hutcheon, I.D., and Banfield, J.F. (2007) Extracellular proteins limit the dispersal of biogenic nanoparticles. *Science* **316:** 1600–1603.

Murray, K.J., and Tebo, B.M. (2007) Cr(III) is indirectly oxidized by the Mn(II)-Oxidizing bacterium *Bacillus* sp. strain SG-1. *Environ Sci Technol* **41:** 528–533.

Murray, K.J., Webb, S.M., Bargar, J.R., and Tebo, B.M. (2007) Indirect oxidation of Co(II) in the presence of the marine Mn(II)-oxidizing bacterium *Bacillus* sp. strain SG-1. *Appl Environ Microbiol* **73:** 6905–6909.

Nealson, K.H., and Saffarini, D. (1994) Iron and manganese in anaerobic respiration – environmental significance, physiology, and regulation. *Annu Rev Microbiol* **48:** 311–343.

Neretin, L.N., Pohl, C., Jost, G., Leipe, T., and Pollehne, F. (2003) Manganese cycling in the Gotland Deep, Baltic Sea. *Mar Chem* **82:** 125–143.

Nico, P.S., Anastasio, C., and Zasoski, R.J. (2002) Rapid photo-oxidation of Mn(II) mediated by humic substances. *Geochim Cosmochim Acta* **66:** 4047–4056.

O'Donnell, V.B., Tew, D.G., Jones, T.G.E., and England, P.J. (1993) Studies on the inhibitory mechanism of iodonium compounds with special reference to neutrophil NADPH oxidase. *Biochem J* **290:** 41–49.

Perfil'ev, B.V., and Gabe, D.R. (1961) *The Capillary Methods of Studying Microorganisms* [in Russian]. Moscow, Russia: Izdatel'stvo Akademii Nauk SSSR.

Petkov, V., Ren, Y., Saratovsky, I., Pasten, P., Gurr, S.J., Hayward, M.A., *et al*. (2009) Atomic-scale structure of biogenic materials by total X-ray diffraction: a study of bacterial and fungal MnO(x). *ACS Nano* **3:** 441–445.

Ravel, B., and Newville, M. (2005) ATHENA, ARTEMIS, HEPHAESTUS: data analysis for X-ray absorption spectroscopy using IFEFFIT. *J Synchrotron Radiat* **12:** 537–541.

Santelli, C.M., Pfister, D.H., Lazarus, D., Sun, L., Burgos, W.D., and Hansel, C.M. (2010) Promotion of Mn(II) oxidation and remediation of coal mine drainage in passive treatment systems by diverse fungal and bacterial communities. *Appl Environ Microbiol* **76:** 4871–4875.

Santelli, C.M., Webb, S.M., Dohnalkova, A.C., and Hansel, C.M. (2011) Diversity of Mn oxides produced by Mn(II)-oxidizing fungi. *Geochim Cosmochim Acta* **75:** 2762–2776.

Saratovsky, I., Gurr, S.J., and Hayward, M.A. (2009) The structure of manganese oxide formed by the fungus *Acremonium* sp strain KR21-2. *Geochim Cosmochim Acta* **73:** 3291–3300.

Sayer, J.A., Kierans, M., and Gadd, G.M. (1997) Solubilisation of some naturally occurring metal-bearing minerals, limescale and lead phosphate by *Aspergillus niger*. *FEMS Microbiol Lett* **154:** 29–35.

Schlosser, D., and Hofer, C. (2002) Laccase-catalyzed oxidation of $Mn^{2+}$ in the presence of natural $Mn^{3+}$ chelators as a novel source of extracellular $H_2O_2$ production and its impact on manganese peroxidase. *Appl Environ Microbiol* **68:** 3514–3521.

Scott, B., and Eaton, C.J. (2008) Role of reactive oxygen species in fungal cellular differentiations. *Curr Opin Microbiol* **11:** 488–493.

Semighini, C.P., and Harris, S.D. (2008) Regulation of apical dominance in *Aspergillus nidulans* hyphae by reactive oxygen species. *Genetics* **179:** 1919–1932.

Sterflinger, K. (2000) Fungi as geologic agents. *Geomicrobiol J* **17:** 97–124.

Stone, A.T., and Morgan, J.J. (1984) Reduction and dissolution of manganese(III) and manganese(IV) oxides by organics. 1. Reaction with hydroquinone. *Environ Sci Technol* **18:** 450–456.

Sunda, W.G., and Kieber, D.J. (1994) Oxidation of humic substrances by manganese oxides yields low-molecular-weight organic substrates. *Nature* **367:** 62–64.

Takemoto, D., Tanaka, A., and Scott, B. (2007) NADPH oxidases in fungi: diverse roles of reactive oxygen species in fungal cellular differentiation. *Fungal Genet Biol* **44:** 1065–1076.

Tebo, B.M., Bargar, J.R., Clement, B.G., Dick, G.J., Murray, K.J., Parker, D., *et al*. (2004) Biogenic manganese oxides: properties and mechanisms of formation. *Annu Rev Earth Planet Sci* **32:** 287–328.

Tebo, B.M., Johnson, H.A., McCarthy, J.K., and Templeton, A.S. (2005) Geomicrobiology of manganese(II) oxidation. *Trends Microbiol* **13:** 421–428.

de la Torre, M.A., and Gomez-Alarcon, G. (1994) Manganese and iron oxidation by fungi isolated from building stone. *Microb Ecol* **27:** 177–188.

Villalobos, M., Toner, B., Bargar, J., and Sposito, G. (2003) Characterization of the manganese oxide produced by *Pseudomonas putida* strain MnB1. *Geochim Cosmochim Acta* **67:** 2649–2662.

Wariishi, H., Valli, K., and Gold, M.H. (1992) Manganese(II) oxidation by manganese peroxidase from the basidiomycete *Phanerochaete chrysosporium* – kinetic mechanism and role of chelators. *J Biol Chem* **267:** 23688–23695.

Webb, S.M. (2005) SIXpack: a graphical user interface for XAS analysis using IFEFFIT. *Phys Scripta* **T115:** 1011–1014.

Webb, S.M. (2006) *SMAK: Sam's Microprobe Analysis Kit, V.0.25*. Menlo Park, CA, USA: Stanford Synchrotron Radiation Laboratory.

Webb, S.M., Tebo, B.M., and Bargat, J.R. (2005) Structural characterization of biogenic Mn oxides produced in seawater by the marine *Bacillus* sp. strain SG-1. *Am Mineral* **90:** 1342–1357.

Wei, Z., Hillier, S., and Gadd, G.M. (2012) Biotransformation of manganese oxides by fungi: solubilization and production of manganese oxalate biominerals. *Environ Microbiol* **14:** 1744–1752.

Zafiriou, O.C., Voelker, B.M., and Sedlak, D.L. (1998) Chemistry of the superoxide radical (O-2(-)) in seawater: reactions with inorganic copper complexes. *J Phys Chem A Mol Spectrosc Kinet Environ Gen Theory* **102:** 5693–5700.

## Supporting information

Additional Supporting Information may be found in the online version of this article:

**Fig. S1.** SEM images showing the surface features of rhodochrosite crystals after reaction with (A) no fungi (control sample), (B) *Pyrenochaeta* sp. DS3sAY3a and (C and D) *Stagonospora* sp. SRC1lsM3a. In contrast to the control sample, in the presence of fungi, extensive surface etching of the $MnCO_3$ surface is evident both within dissolution pits and on basal surfaces.

**Fig. S2.** SEM images showing *Stagonospora* sp. SRC1lsM3a hyphae growing into cracks (A and B) and dissolution pits (C) on the surface of rhodochrosite crystals.

**Fig. S3.** SEM images showing organic coatings on rhodochrosite crystals after reaction with (A and B) *Pithomyces chartarum* DS1bioJ1b and (C) *Pleosporales* sp. AP3s5JAC2b.

**Fig. S4.** Bulk EXAFS of Mn oxides formed following Mn(II) oxidation of $MnCO_3$ by fungal species A–F (see Table 1 for species name). Three reference compounds needed to reconstruct the mycogenic oxides by linear combination fitting (LCF) are included in gray. Data are shown in solid lines and fits in dotted lines. Fitting results and parameters are listed in Table 1.

**Fig. S5.** Stereomicroscope images showing the impact of chemical/enzyme inhibitors on Mn oxide formation by *Pyrenochaeta* sp. DS3sAY3a (A–D) and *Stagonospora* sp. SRC1lsM3a (E–H). All images depict fungal hyphae and Mn oxides on AY agar plates after approximately 2 weeks of growth.

A and E. AY agar controls amended with 200 μM Mn(II). Brown colour indicates mycogenic Mn oxides.

B and F. Cells grown with 200 μM Mn(II) and 25 μM (B) or 10 μM (F) DPI, an inhibitor of NADPH oxidases.

C and G. Cells grown with 200 μM Mn(II) and 200 μM Cu(II), a scavenger of superoxide.

D and H. Cells grown with 200 μM Mn(II) and 200 μM Zn(II). Zn(II) imparts a similar level of toxicity as Cu(II) but does not react with superoxide.

**Fig. S6.** Mycogenic Mn oxide samples were analysed with micro-Fourier transform infrared spectroscopy (μ-FTIR). (Above) Mn oxide clusters in cultures of *Pyrenochaeta* sp. DS3sAY3a. The Mn oxides were not associated with any cellular materials. Clusters were gently removed from the medium with sterile wooden inoculation sticks, washed six times in distilled water and dissolved with 20 mM ascorbic acid to liberate organics from Mn oxides prior to analysis. Samples were analysed on a μ-FTIR at Bruker Optics (Billerica, MA, USA) in reflectance mode. These preliminary μ-FTIR data are promising in that they indicate the presence of organics directly associated with cell-free Mn oxide clusters.